

# Characteristic times for the Fermi-Ulam Model

Joelson D. Veloso Hermes<sup>1,2</sup>, Edson D. Leonel<sup>2</sup>

<sup>1</sup>Instituto Federal de Educação, Ciência e Tecnologia do Sul de Minas Gerais - IFSULDEMINAS, Inconfidentes - Brazil  
<sup>2</sup>Departamento de Física, UNESP - Univ. Estadual Paulista, Av.24A, 1515 - Bela Vista - 13506-900 - Rio Claro - SP - Brazil

---

## Abstract

The mean Poincaré recurrence time as well as the Lyapunov time are measured for the Fermi-Ulam model. We confirm the mean recurrence time is dependent on the size of the window chosen in the phase space to where particles are allowed to recur. The fractal dimension of the region is determined by the slope of the recurrence time against the size of the window and two numerical values were measured: (i)  $\mu = 1$  confirming normal diffusion for chaotic regions far from periodic domains and; (ii)  $\mu = 2$  leading to anomalous diffusion measured near periodic regions, a signature of local trapping of an ensemble of particles. The Lyapunov time is measured over different domains in the phase space through a direct determination of the Lyapunov exponent, indeed being defined as its inverse.

*Key words:* Chaos; Diffusion; Poincaré Recurrence.

---

## 1. Introduction

Diffusion of particles has intrigued scientists of different areas over the years. Applications are the wider as possible ranging from medicine [1] where a specific medical or chemical drug diffuses in blood to reach its destiny, water infiltration [2] in the surface of the planet caring chemical elements from pesticides to the water table, pollen diffusion of plants [3], pollution in air [4] or in water [5] and many others. In dynamical systems diffusion can be treated as via the solution of the diffusion equation [6] leading to results proving scaling invariance in chaotic systems [7]. Moreover, diffusion in Hamiltonian systems is also connected to Poincaré recurrence [8] which is defined as the time a particle spends moving along the phase space to return to a specific region to where it has passed earlier. It is known [9] that such a time obeys specific laws that confirm the existence of stickiness [10] and hence anomalous diffusion [11] or normal diffusion [12].

Whenever observing stickiness, chaotic dynamics is also present. One of the basic tools to measure chaotic properties in nonlinear systems is the Lyapunov exponent  $\lambda$  [13]. It is based on the average separation in time of two nearby initial conditions. A characteristic time associated with it [14] is the Lyapunov time  $t_L = 1/\lambda$ . Moreover in Hamiltonian chaos the Liouville's theorem [15] warrants area preservation in the phase space. In mixed systems where chaos coexists with periodic islands and invariant tori in the phase space, a particle in the chaotic domain can not cross through the invariant tori nor get into the islands. This implies that once in the chaos, always in the chaos. It also yields in to an important property that a given particle may recur to a certain region in the phase space and

that the time it spends to return to a specific domain is called as Poincaré recurrence time  $t_r$ . This characteristic time depends on the size of the region and on the type of the dynamics nearby it. The slope of the curve given by  $t_r$  plotted against the size of the region gives the fractal dimension of the set of points of such a region and marks the kind of diffusion measured. In this paper we revisit the Fermi-Ulam model [16] and we are seeking to understand and describe the behavior of the two characteristic times mentioned above, namely the Lyapunov and the Poincaré recurrence times.

The model is composed of a particle confined to move inside of two rigid walls where one of them is fixed while the other one moves periodically in time. Collisions are assumed to be elastic in the sense that there is no lose of energy upon the impacts, hence the area of the phase space is preserved. When the particle has very low energy<sup>1</sup> the elapsed time between impacts is large. Hence there is no correlation between the phase of the moving wall at the impact  $n$  as compared to the phase at the impact  $(n + 1)$ . The absence of correlation between phases leads the velocity of the particle to grow. For the low energy regime a particle exhibits chaotic dynamics while with the growth of the velocity correlations between phases appear producing regularity in the phase space where islands of stability as well as invariant tori are observed. The lowest energy invariant spanning curve has crucial importance in limiting the size of the chaotic sea preventing the unlimited diffusion of the chaotic dynamics. This unlimited diffusion was believed to be observed in dynamical systems produced by collisions of an ensemble of particles with moving periodic boundary leading to a phenomena called as Fermi acceleration. The existence of the invariant spanning

---

<sup>1</sup>We mention as very low when the energy of the particle is comparable with the energy of the moving wall, i.e., the velocity of the particle has the same magnitude of the maximum velocity of the moving wall.

---

*Email address:* joelson.hermes@ifsuldeminas.edu.br,  
Phone: +55 35 3464 1200 (Joelson D. Veloso Hermes<sup>1,2</sup>)

curve prevent this unlimited growth. It also imposes an interesting scaling invariance of the chaotic sea [17] near a transition from integrability to non integrability [18].

The paper is organized as follows. In Section 2 we discuss the mapping and the properties of the phase space. Some properties of the Lyapunov exponent as well as the Lyapunov time are discussed in Section 3. The Poincaré recurrence time is discussed in Section 4 while discussions and final remarks are drawn in Section 5.

## 2. The model, the mapping and the phase space

The Fermi-Ulam model is composed of a classical particle confined to move inside of two rigid walls. One is considered fixed at  $x = \ell$  while the other is periodically moving whose position is given by  $x_w(t) = X_0 \cos(\omega t)$  where  $X_0$  is the amplitude of the motion and  $\omega$  is the frequency of oscillation. The particle experiences elastic collisions with the wall. The dynamics of the particle is given by a two dimensional, nonlinear and area preserving mapping describing how the velocity of the particle and phase of the moving wall transform from the impact  $n$  to the impact  $n+1$ . The version of the model we consider in this paper is the so called static wall approximation [19]. It assumes that, because of the small range of values considered for the control parameter  $X_0$ , both walls are considered fixed. However when a particle collides with one wall at the left it suffers an exchange of energy and momentum as if the wall were moving. This version of the model retains the majority of the properties of the whole version where the moving wall is taking into account, including localization of the periodic regions, determination of the position of the invariant spanning curves and the scaling produced by it [17]. However there is a huge advantage of speeding up the numerical simulations the static wall approximation has as compared to the complete model where transcendental equations are compulsory to be solved.

Considering a set of dimensionless variables such as  $\varepsilon = X_0/\ell$ ,  $V_n = v_n/(\omega\ell)$  with  $v_n$  representing the velocity of the particle and  $\phi = \omega t$  the mapping describing the dynamics of the model is written as

$$T : \begin{cases} \phi_{n+1} = \left[ \phi_n + \frac{2}{V_n} \right] \bmod 2\pi \\ V_{n+1} = |V_n - 2\varepsilon \sin(\phi_{n+1})| \end{cases}, \quad (1)$$

where the absolute value in the second equation was introduced as an attempt to avoid that, after a collision, a particle has negative velocity [20].

The phase space of the model is shown in Figure 1 for the control parameter  $\varepsilon = 10^{-3}$ . It is easy to note a mixed structure of it including the presence of a large chaotic region co-existing with periodic structures such as elliptical islands and also invariant spanning curves. There are four regions in the phase space identified in the figure corresponding to the domains we are considering in the investigation along this paper. The size of the chaotic sea is marked by the minimal region as the lowest velocity of the wall while the upper limit is determined by the smallest velocity energy invariant spanning curve. Above the curve one observe local chaos while below of it there

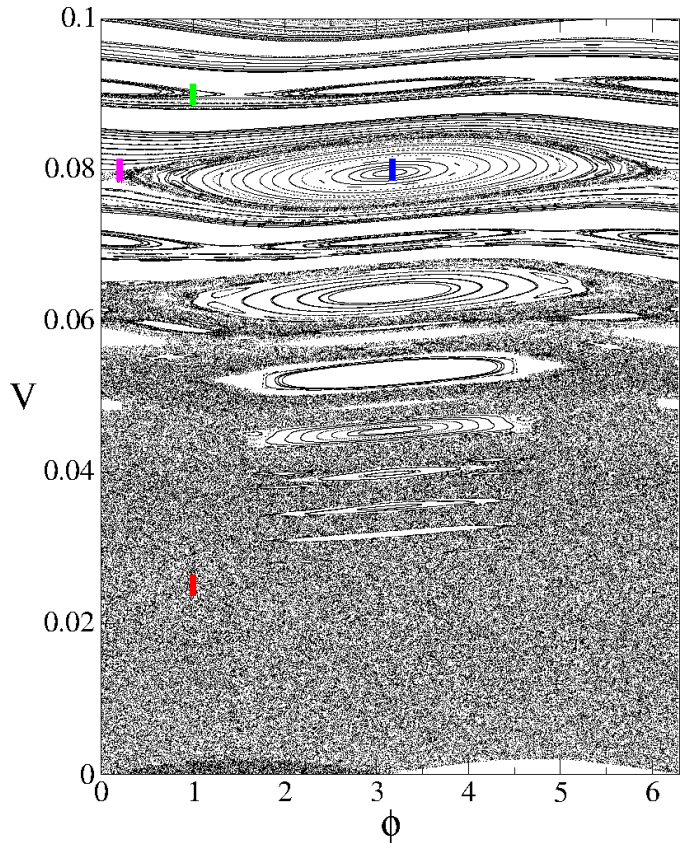


Figure 1: Plot of the phase space for the static wall approximation of the Fermi-Ulam Model. The control parameter used was  $\varepsilon = 10^{-3}$ .

is global chaos. According to the Chirikov criteria [8], the last invariant spanning curve broken in the so called Standard Mapping [8] happens at a critical parameter  $K_c \cong 0.9716\dots$ . The standard mapping is written as  $I_{n+1} = I_n + K \sin(\theta_{n+1})$  and  $\theta_{n+1} = (\theta_n + I_n) \bmod 2\pi$ . When the second equation of the mapping (1) is written replacing  $V_n = V^* + \Delta V_n$  with  $(\Delta V)/V^* \ll 1$  and Taylor expanding it till first order and that when compared with the equations of the standard mapping leads to  $V^* = \frac{2}{\sqrt{0.9716\dots}} \sqrt{\varepsilon}$ . The exponent heading  $\varepsilon$  plays a major rule on the regime of growth and saturation of the curves for the average velocity. As discussed in Ref. [17], the exponent of the curves of  $\bar{V}_{\text{sat}} \propto \varepsilon^\alpha$  with  $\alpha = 1/2$  which is one of the three critical exponents. The exponent marking the diffusion for low velocity is  $V \propto (n\varepsilon^2)^\beta$  with  $\beta = 1/2$ . The last exponent is obtained by a scaling law  $z = \alpha/\beta - 2$ .

In the next section we discuss the characteristic Lyapunov time based on the results for the positive Lyapunov exponent.

## 3. The Lyapunov Time

In this section we discuss our results for the characteristic Lyapunov time, which is defined as the inverse of the positive Lyapunov exponent. Indeed the Lyapunov exponent is a common measure to estimate how chaotic a system is. A positive Lyapunov exponent yields in an exponentially fast spread of

two very near initial conditions in the phase space. For a two dimensional mapping they can be obtained [21] using the eigenvalues of the Jacobian matrix

$$\lambda_j = \lim_{n \rightarrow \infty} \frac{1}{n} \ln |\Lambda_n^{(j)}|, \quad (2)$$

with  $j = 1, 2$  where  $\Lambda_n^{(j)}$  correspond to the eigenvalue of the Jacobian matrix  $M = \prod_{i=1}^n J_i(V_i, \phi_i) = J_n J_{n-1} J_{n-2} \dots J_2 J_1$ . Since the convergence of the Lyapunov exponent is observed for large  $n$  the accumulation of the product of the  $J_i$  matrices may lead to overflow in their coefficients hence making hard the estimation of  $\lambda$ . The triangularization algorithm avoid such a trouble. It consists of rewrite  $J$  as  $J = \Theta T$  with  $\Theta$  being an orthogonal matrix obeying the property of  $\Theta^{-1} = \Theta^T$  and  $T$  is a triangular matrix. Therefore this leads to

$$\Theta = \begin{pmatrix} \cos(\theta) & -\sin(\theta) \\ \sin(\theta) & \cos(\theta) \end{pmatrix},$$

with

$$T = \begin{pmatrix} T_{11} & T_{12} \\ 0 & T_{22} \end{pmatrix}.$$

We notice the matrix  $M$  can be written as

$$\begin{aligned} M &= J_n J_{n-1} J_{n-2} \dots J_2 J_1, \\ &= J_n J_{n-1} J_{n-2} \dots J_2 \Theta_1 \Theta_1^{-1} J_1. \end{aligned} \quad (3)$$

Defining  $T_1 = \Theta_1^{-1} J_1$  and  $\tilde{J}_2 = J_2 \Theta_1$  the coefficients of  $T_1$  are

$$\begin{pmatrix} T_{11} & T_{12} \\ 0 & T_{22} \end{pmatrix} = \begin{pmatrix} \cos(\theta) & \sin(\theta) \\ -\sin(\theta) & \cos(\theta) \end{pmatrix} \begin{pmatrix} j_{11} & j_{12} \\ j_{21} & j_{22} \end{pmatrix}.$$

From  $T_{21} = 0$  we end up with  $0 = -j_{11} \sin(\theta) + j_{21} \cos(\theta)$  yielding in

$$\frac{j_{21}}{j_{11}} = \frac{\sin(\theta)}{\cos(\theta)}. \quad (4)$$

Instead of using  $\theta = \arctan(j_{21}/j_{11})$  which is rather expensive numerical function, we use the expressions of  $\sin(\theta)$  and  $\cos(\theta)$  directly from  $J$ , hence

$$\cos(\theta) = \frac{j_{11}}{\sqrt{j_{11}^2 + j_{21}^2}}, \quad (5)$$

$$\sin(\theta) = \frac{j_{21}}{\sqrt{j_{11}^2 + j_{21}^2}}. \quad (6)$$

The expressions for  $T_{11}$  and  $T_{22}$  can be written as  $T_{11} = j_{11} \cos(\theta) + j_{21} \sin(\theta)$  and also  $T_{22} = -j_{12} \sin(\theta) + j_{22} \cos(\theta)$  producing the following expressions

$$T_{11} = \frac{j_{11}^2 + j_{21}^2}{\sqrt{j_{11}^2 + j_{21}^2}}, \quad (7)$$

$$T_{22} = \frac{j_{11} j_{22} - j_{12} j_{21}}{\sqrt{j_{11}^2 + j_{21}^2}}. \quad (8)$$

Once  $T_{11}$  and  $T_{22}$  are known the matrix  $\tilde{J}_2$  is given by  $\tilde{J}_2 = J_2 \Theta_1$

$$\begin{pmatrix} \tilde{j}_{11} & \tilde{j}_{12} \\ \tilde{j}_{21} & \tilde{j}_{22} \end{pmatrix} = \begin{pmatrix} j_{11} & j_{12} \\ j_{21} & j_{22} \end{pmatrix} \begin{pmatrix} \cos(\theta) & -\sin(\theta) \\ \sin(\theta) & \cos(\theta) \end{pmatrix}.$$

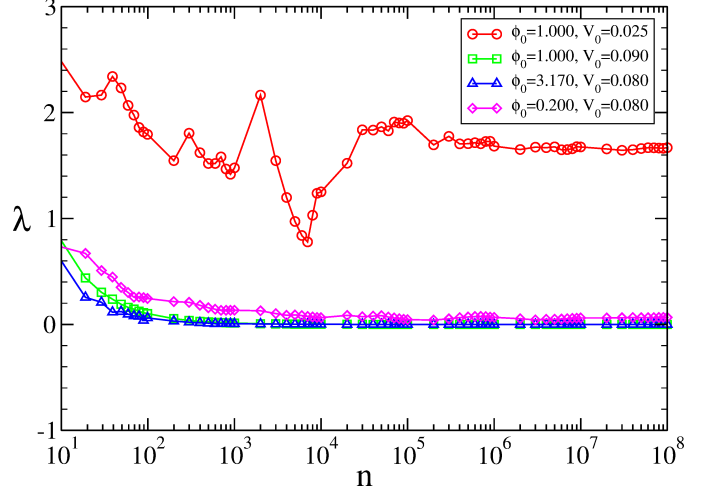


Figure 2: Plot of the time evolution of the positive Lyapunov exponent for the regions marked in the phase space of figure 1. The control parameter used was  $\varepsilon = 10^{-3}$ . Each initial condition was evolved up to  $n = 10^8$  collisions with the walls.

The procedure is then repeated for the second iteration, and third and any further iteration of the mapping until the complete series of matrices is exhausted. The Lyapunov exponents are then given by

$$\lambda_j = \lim_{n \rightarrow \infty} \sum_{i=1}^n \ln |T_{jj}^{(i)}|, \quad j = 1, 2. \quad (9)$$

Figure 2 shows the converge of the positive Lyapunov exponent using the algorithm discussed above for the specific regions defined in the phase space. Region 1 is marked as the red color in the Figure and is evolved from the initial condition ( $\phi_0 = 1.000, V_0 = 0.025$ ), while region 2 marked as green is for ( $\phi_0 = 1.000, V_0 = 0.090$ ), blue is for region 3 with ( $\phi_0 = 3.170, V_0 = 0.080$ ) and finally magenta is for region 4 obtained for ( $\phi_0 = 0.200, V_0 = 0.080$ ). A chaotic domain leads to a convergence of  $\bar{\lambda} = 1.665(3)$  while periodic regions lead to Lyapunov exponent converging to null value. Table 1 summarizes both the Lyapunov exponent as well as the Lyapunov time which is defined as the inverse of the Lyapunov exponent  $t_L = 1/\lambda$ . It is important to notice that for the chaotic regions ( $R_1$  and  $R_4$ ) the Lyapunov time is relatively short, so returning to Lyapunov time concept it is clear that for these regions the map quickly shows a chaotic behavior. However for the regions near the islands of stability ( $R_2$  and  $R_3$ ) the Lyapunov time is significantly large indicating absence of chaos. We emphasize both  $\lambda$  and  $t_L$  were calculated for a finite number of iterations of  $10^8$ .

Figure 4 shows a plot of  $t_L$  vs.  $\varepsilon$ . Each point of the curve was obtained after a long simulation of  $10^8$  iterations for the calculation of  $\lambda$ . One sees that  $t_L$  increases, in the average, with the increase of  $\varepsilon$ . The regime of growth for  $t_L$  is slow at the beginning and speeds up for  $\varepsilon > 10^{-1}$ . The latter window of control parameter the static wall approximation has severe limitations since the movement of the time dependent wall would

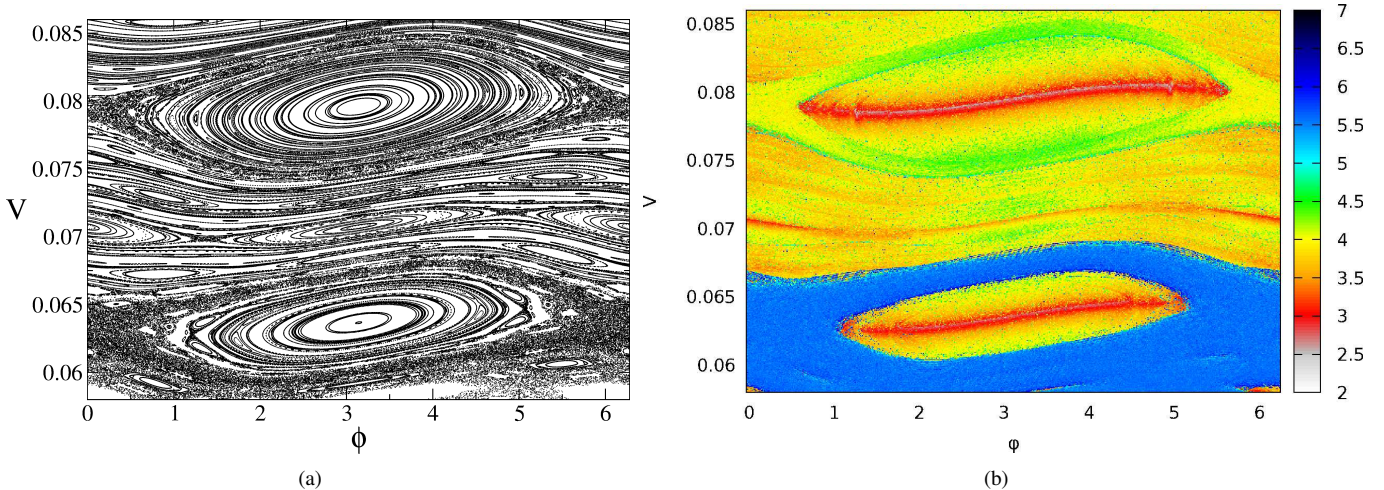


Figure 3: (a) Plot of an expanded region of the phase space shown in Fig. 1 where the two largest islands are observed, one below and other above the first invariant spanning curve. (b) Plot of the same region of (a) with the color scale representing in logarithmic scale the mean Poincaré recurrence time  $\langle t_r \rangle$ .

Table 1: Numerical values of  $\lambda$  and  $t_L$  for the regions indicated in the phase space of the figure 1.

Regions	$\lambda$	$t_L = 1/\lambda$
$R_1$	1.665(3)	0.600(1)
$R_2$	$1.598(1) \times 10^{-6}$	$62(5) \times 10^5$
$R_3$	$4.258(3) \times 10^{-7}$	$2348(4) \times 10^3$
$R_4$	$6.627(4) \times 10^{-2}$	15.089(9)

indeed affects the shape of the phase space leading to frequent non physical situations.

#### 4. The Poincaré Recurrence Time

In this section we discuss the Poincaré recurrence time. The essence is simple and consists in determine the time a particle which left a given region of the phase space returns to a point  $\delta$ -close to that region. An orbit in the phase space is said to recur to an  $I_\delta$  interval if, once it starts at point  $\vec{x}_0 \in I_\delta$ ,  $\forall \delta$  with  $\vec{x}_0 = (V_0, \phi_0)$  there is a time  $t^*$  such that, after  $t^*$ , the orbit is at a distance  $|\vec{x}_{t^*} - \vec{x}_0| \leq \delta$ , hence  $\vec{x}_{t^*} \in I_\delta$  (see Ref. [22]). Figure 3(a) shows an expanded domain of the phase space plotted in Figure 1 where two period-1 islands are present being one below and another above of the first invariant spanning curve. We notice also that in between them there is a chain of smaller islands and some chaotic regions around them hence characteristic of a mixed phase space. Figure 3(b) plots the same region of Figure 3(a) but with the color scheme defined as the mean Poincaré recurrence time  $\langle t_r \rangle$  plotted in logarithmic scale. From figure 3(b) it is possible to notice a separation of two regions of the phase space, one in blue (dark gray) indicating that  $\langle t_r \rangle$  is between  $10^5$  and  $10^6$  while in the second, in orange (light gray), giving  $\langle t_r \rangle$  between  $10^3$  and  $10^4$  iterations. It is worth mentioning that the stickiness phenomenon can affect the recurrence time. This is because the orbit stays stuck in the certain region

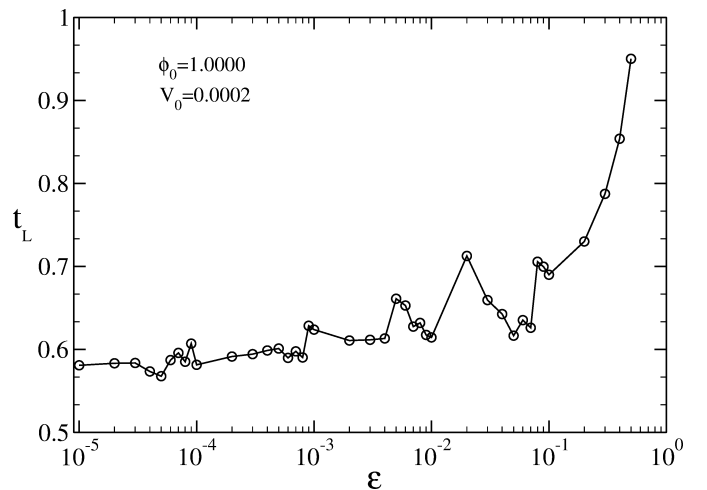


Figure 4: Plot of the numerical value of  $t_L$  as a function of  $\epsilon$  measured for a chaotic region of the phase space.

of the phase space until it escapes such domain and eventually returns to a position close to the initial condition. This can be confirmed looking at figure 3(b) and seeing that near the islands where stickiness is observed the recurrence time is longer as compared to other regions and clearly identified in the color scale.

Other interesting physical measure from the Poincaré recurrence time is linked to the fractal dimension of the region since a power law fitting of  $\langle t_r \rangle$  vs.  $\epsilon$  gives an exponent which is the absolute value of the fractal dimension  $d_w$  whenever the limit of  $\epsilon \rightarrow 0$  is considered [23]. The parameter  $\epsilon$  corresponds to the size of the recurrent window in the phase space. The relationship between  $t_r$  and the chosen region is given as

$$\langle t_r \rangle = \frac{1}{\epsilon^{d_w}}, \quad (10)$$

where  $d_w$  is the fractal dimension and  $\epsilon$  the side of the box [23].

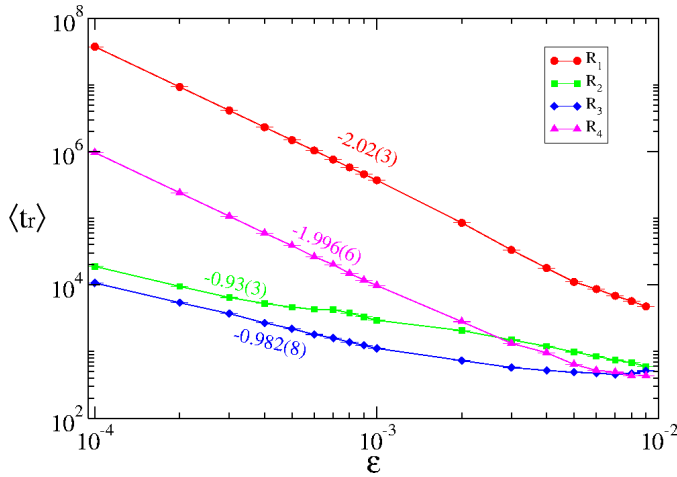


Figure 5: Plot of the average Poincaré recurrence time  $\langle t_r \rangle$  as a function of the size of the recurrence interval  $\epsilon$ , for the different regions indicated in figure 1.

It is shown in figure 5 a plot of  $\langle t_r \rangle$  vs.  $\epsilon$  where two different slopes are observed. For the curves related to the initial conditions given in the chaotic regions a power law fitting gives a decay with slope  $\approx -2$  while for the initial conditions given in the regions on the periodic islands the slope of the decay is  $\approx -1$ . The fractal dimension is related to the diffusion coefficient  $\mu$  through the following equation [23]

$$d_w = \frac{2}{\mu}. \quad (11)$$

When the initial conditions are located along the islands of periodicity,  $d_w = 1$  yielding  $\mu = 2$  which is a signature of anomalous diffusion. On the other hand for initial conditions placed in the chaotic region,  $d_w = 2$  leading to  $\mu = 1$  and one observed the chaotic orbits experience normal diffusion.

## 5. Discussion and Final remarks

Let us now discuss the implications of the results obtained. Unlike to what happens for the standard map where the Lyapunov exponent  $\lambda$  increases as the nonlinearity increases [23], in the Fermi-Ulam model the Lyapunov exponent decreases and consequently, the Lyapunov  $t_L$  time increases with the increase of the nonlinearity. This is due to the fact that in the standard map the increase in the nonlinearity parameter causes the invariant curves and stable structures to be destroyed and chaos dominate over the system, whereas in the Fermi-Ulam model, the increase in the nonlinearity does not break the invariant spanning curve. Chaotic sea is scaling with the localization of the first invariant spanning curve hence of the type  $\sqrt{\epsilon}$ .

Regarding the Poincaré recurrence time  $t_r$  the results found by [23] for the standard map were also observed in the Fermi-Ulam model confirming  $\langle t_r \rangle$  scales with  $\epsilon$  which is the size of the recurrence domain. For chaotic regions the slope obtained is about  $\mu = 2$  while for periodic regions is  $\mu = 1$ .

As a final remark, we have measured both the Lyapunov  $t_L$  time as the inverse of the Lyapunov exponent for different regions of the phase space. The average Poincaré recurrence was confirmed to be dependent on the size of the recurrent window and where the initial condition was given. A power law fitting of  $\langle t_r \rangle$  vs.  $\epsilon$  gives a slope of  $-2$  for initial conditions taken in chaotic region while yields a slope of  $-1$  for periodic domains. We saw that  $d_w = \frac{2}{\mu}$ , so that in the chaotic regions the diffusion exponent converges to  $\mu = 1$  and within the stability islands  $\mu = 2$ .

## ACKNOWLEDGMENTS

Instituto Federal de Educação, Ciência e Tecnologia do Sul de Minas Gerais, IFSULDEMINAS - Campus Inconfidentes. Grupo de Escudos em Modelagem Computacional e Aplicações - GEMCA. EDL thanks to CNPq (301318/2019-0) and FAPESP (2019/14038-6), Brazilian agencies.

## References

- [1] Kenya Murase, Shuji Tanada, Hiroshi Mogami, Masashi Kawamura, Masao Miyagawa, Masafumi Yamada, Hiroshi Higashino, Atsushi Iio, and Ken Hamamoto. Validity of microsphere model in cerebral blood flow measurement using n-isopropyl-p-(i-123) iodoamphetamine. *Medical physics*, 17(1):79–83, 1990.
- [2] C Hagedorn, EL Mc Coy, and TM Rahe. The potential for ground water contamination from septic effluents 1. *Journal of Environmental Quality*, 10(1):1–8, 1981.
- [3] William F Morris. Predicting the consequence of plant spacing and biased movement for pollen dispersal by honey bees. *Ecology*, 74(2):493–500, 1993.
- [4] David Popp. International innovation and diffusion of air pollution control technologies: the effects of nox and so2 regulation in the us, japan, and germany. *Journal of Environmental Economics and Management*, 51(1):46–71, 2006.
- [5] Rostislav Vsevolodovich Ozmidov. Diffusion of contaminants in the ocean. 1990.
- [6] Venkataraman Balakrishnan. *Elements of nonequilibrium statistical mechanics*, volume 3. Ane Books, 2008.
- [7] Edson D. Leonel and Chia M. Kuwana. An investigation of chaotic diffusion in a family of hamiltonian mappings whose angles diverge in the limit of vanishingly action. *Journal of Statistical Physics*, 170:69–78, 2018.
- [8] A.J. Lichtenberg and M.A. Leiberman. *Regular and chaotic dynamics*. Applied mathematical sciences. Springer-Verlag, 1992.
- [9] Mirella Harsoula and George Contopoulos. Global and local diffusion in the standard map. *Physical Review E*, 97(2):022215, 2018.
- [10] Eduardo G Altmann, Adilson E Motter, and Holger Kantz. Stickiness in mushroom billiards. *Chaos: An Interdisciplinary Journal of Nonlinear Science*, 15(3):033105, 2005.
- [11] Leonid A Bunimovich. Fine structure of sticky sets in mushroom billiards. *Journal of Statistical Physics*, 154(1-2):421–431, 2014.
- [12] George M Zaslavsky. *The physics of chaos in Hamiltonian systems*. world scientific, 2007.
- [13] Arkady Pikovsky and Antonio Politi. *Lyapunov exponents: a tool to explore complex dynamics*. Cambridge University Press, 2016.
- [14] Henry E. Kandrup, Christos Siopis, G. Contopoulos, and Rudolf Dvorak. Diffusion and scaling in escapes from two-degrees-of-freedom hamiltonian systems. *Chaos: An Interdisciplinary Journal of Nonlinear Science*, 9(2):381–392, 1999.
- [15] F. Reif. *Fundamentals of statistical and thermal physics* / [by] F. Reif. McGraw-Hill Kogakusha Tokyo, international student ed. edition, 1965.
- [16] ENRICO Fermi. On the origin of the cosmic radiation. *Phys. Rev.*, 75:1169–1174, Apr 1949.
- [17] E. D. Leonel and P. V. E. McClintock. Chaotic properties of a time-modulated barrier. *Phys. Rev. E*, 70:016214, Jul 2004.

- [18] Edson D Leonel, Juliano A de Oliveira, and Farhan Saif. Critical exponents for a transition from integrability to non-integrability via localization of invariant tori in the hamiltonian system. *Journal of Physics A: Mathematical and Theoretical*, 44(30):302001, jul 2011.
- [19] A. K. Karlis, P. K. Papachristou, F. K. Diakonos, V. Constantoudis, and P. Schmelcher. Hyperacceleration in a stochastic fermi-ulam model. *Phys. Rev. Lett.*, 97:194102, Nov 2006.
- [20] Edson Denis Leonel. *Invariância de Escala em Sistemas Dinâmicos Não Lineares*. Blucher, first edition, 2019.
- [21] J. P. Eckmann and D. Ruelle. Ergodic theory of chaos and strange attractors. *Rev. Mod. Phys.*, 57:617–656, Jul 1985.
- [22] Eduardo G. Altmann, Elton C. da Silva, and Iberl L. Caldas. Recurrence time statistics for finite size intervals. *Chaos: An Interdisciplinary Journal of Nonlinear Science*, 14(4):975–981, 2004.
- [23] Mirella Harsoula, Kostas Karamanos, and George Contopoulos. Characteristic times in the standard map. *Physical Review E*, 99(3):032203, 2019.